ORNL/TM--8707

DE83 016932

ORNL/TM-8707
Dist. Category UC-20d

Contract No. W-7405-eng-26

Engineering Physics Division

MONTE CARLO CALCULATIONS OF NEUTRON AND GAMMA-RAY ENERGY SPECTRA FOR FUSION-REACTOR SHIELD DESIGN: COMPARISON WITH EXPERIMENT †

R. T. Santoro
J. M. Barnes*

†Paper presented at the 5th Topical Meeting on the Technology of Fusion Energy, Knoxville, TN, April 26-28, 1983. A version of this Technical Memorandum will be published in a special edition of Nuclear Technology/ Fusion.

*UCC-ND Computer Sciences Division

This Work Sponsored by
Office of Fusion Energy
U. S. Department of Energy

Date Published - August 1983

OAK RIDGE NATIONAL LABORATORY
Oak Ridge, Tennessee 37830
operated by
UNION CARBIDE CORPORATION
for the
DEPARTMENT OF ENERGY

DISCLAIMER

MONTE CARLO CALCULATIONS OF NEUTRON AND GAMMA-RAY ENERGY SPECTRA FOR FUSION REACTOR SHIELD DESIGN: COMPARISON WITH EXPERIMENT

R. T. Santoro and J. M. Barnes

ABSTRACT

Neutron and gamma-ray energy spectra resulting from the interactions of ~14-MeV neutrons in laminated slabs of stainless steel type-304 and borated polyethylene have been calculated using the Monte Carlo code MCNP. The calculated spectra are compared with measured data as a function of slab thickness and material composition and as a function of detector location behind the slabs. Comparisons of the differential energy spectra are made for neutrons with energies above 850 keV and for gamma rays with energies above 750 keV. The measured neutron spectra and those calculated using Monte Carlo methods agree within 5% to 50% depending on the slab thickn. and composition and neutron energy. The agreement between the measured and calculated gamma-ray energy spectra are also within this range. The MCNP data are also in favorable agreement with attenuated data calculated previously by discrete ordinates transport methods and the Monte Carlo code SAM-CE.

I. INTRODUCTION

The nuclear design calculations that are being carried out for fusion reactors use radiation transport methods and cross-section data that have not been verified for this application. Since neutron-producing fusion reactors do not currently exist, this verification is being provided by a program of integral experiments at the Oak Ridge National Laboratory. Measurements of the neutron and gamma-ray energy spectra that result from the reactions of 14-MeV neutrons are being performed for a wide range of materials and in assemblies typical of those proposed for use in fusion reactors. In this paper, neutron and gamma-ray spectra calculated using the Monte Carlo code MCNP[1] are compared with measured spectra as a function of thickness and material composition of laminated slabs of stainless steel type-304 (SS-304) and borated polyethylene (BP). These materials were chosen since they have neutron attenuation properties that are similar to those proposed for use in the shields being designed for the first generation fusion reactors.

The spectra calculated using MCNP are also compared with calculated spectra obtained previously using discrete ordinates methods,[2] and also with calculated neutron spectra obtained by Schmidt and Rose[3] with the Monte Carlo code SAM-CE. The purpose of this calculation, as well as those reported in Refs. 2 and 3, is to verify radiation transport methods and cross-section data in reproducing the neutron and gamma-ray spectra that result from ~14 MeV neutron reactions in fusion reactor shield materials and to determine the adequacy of the codes and nuclear data for the performance of nuclear design calculations for fusion reactors.

A brief description of the experiment is given in Section II. Details of the calculations are given in Section III. The results of this calculation and comparisons between the measured spectra and those calculated in Refs. 2 and 3 are presented and discussed in Section IV.

II. DESCRIPTION OF THE EXPERIMENT

Deuterons are accelerated with an electrostatic generator to a kinetic energy of 250 keV and are focused on a 4-mg/cm^2 thick titanium-tritide target. The deuterons react with the tritium to produce ~14-MeV neutrons via the

$$D + T \rightarrow n + {}^4\mathrm{He} + 17.6\ \mathrm{MeV} \qquad (1)$$

reaction. The target is enclosed in a cylindrical iron can that has the dual function of shaping the neutron spectrum incident on the experiment slabs and of reflecting the neutrons emitted in the backward direction towards the slabs. The iron source can was carefully designed to modify the D-T neutron source distribution to make it characteristic of that incident on the first wall of a fusion reactor.[4]

The neutron- gamma-ray spectra were measured with an NE-213 liquid scintillator. Neutron and gamma-ray events in the detector are separated using pulse-shape discrimination methods and are stored in separate memory locations in a ND-812 pulse-height analyzer/computer. The neutron and gamma-ray pulse-height data were normalized to the absolute neutron yield from the target, which was determined using associated particle counting methods.

The pulse-height data were obtained for neutrons with energies above 850 keV and for gamma rays above 750 keV. The dynamic range of the neutron pulse-height distribution and the nonlinearity of light output from the scintillator limits the detection of neutrons to those with energies above 850 keV. The neutron and gamma-ray pulse-height spectra were unfolded using the program FERD[5] to produce energy spectra. The neutron response matrix was obtained using the pulsed neutron beam from the Oak Ridge Linear Accelerator,[6] and the gamma-ray response matrix was generated using gamma-ray sources of known energies. The energy resolution of the detector varies as

$$R_N = \sqrt{300 + 800/E_N} \tag{2}$$

for neutrons of energy E_N and as

$$R_\gamma = \sqrt{170 + 288/E_\gamma} \tag{3}$$

for gamma rays of energy E_γ. R_N and R_γ are the full width of half maximum (in percent) of the detector response to neutrons or gamma rays, respectively.

Detailed descriptions of the experiment are given in Refs. 2, 3, and 6.

III. DETAILS OF THE CALCULATIONS

The MCNP calculations were carried out using the two-dimensional model of the experimental configuration shown in Fig. 1. The concrete shield-support structure, the source can, and the slab geometries were modeled in r-z geometry with cylindrical symmetry about the beam axis. The neutron and neutron-induced gamma-ray fluences were calculated using point estimators.

Neutrons produced in the D-T reaction have an angle-energy dependence that must be accounted for in the calculations to assure that the measured and calculated neutron and gamma-ray spectra are compared to the same neutron source. The neutron and gamma-ray spectra were calculated with MCNP in two steps: first, by sampling from neutrons emitted from the target into the polar angular interval between 0 to 40° (forward calculation) and then by sampling from neutrons emitted into the angular interval between 40 and 180° (backward calculation). The probabilities for the emission of neutrons into these angular

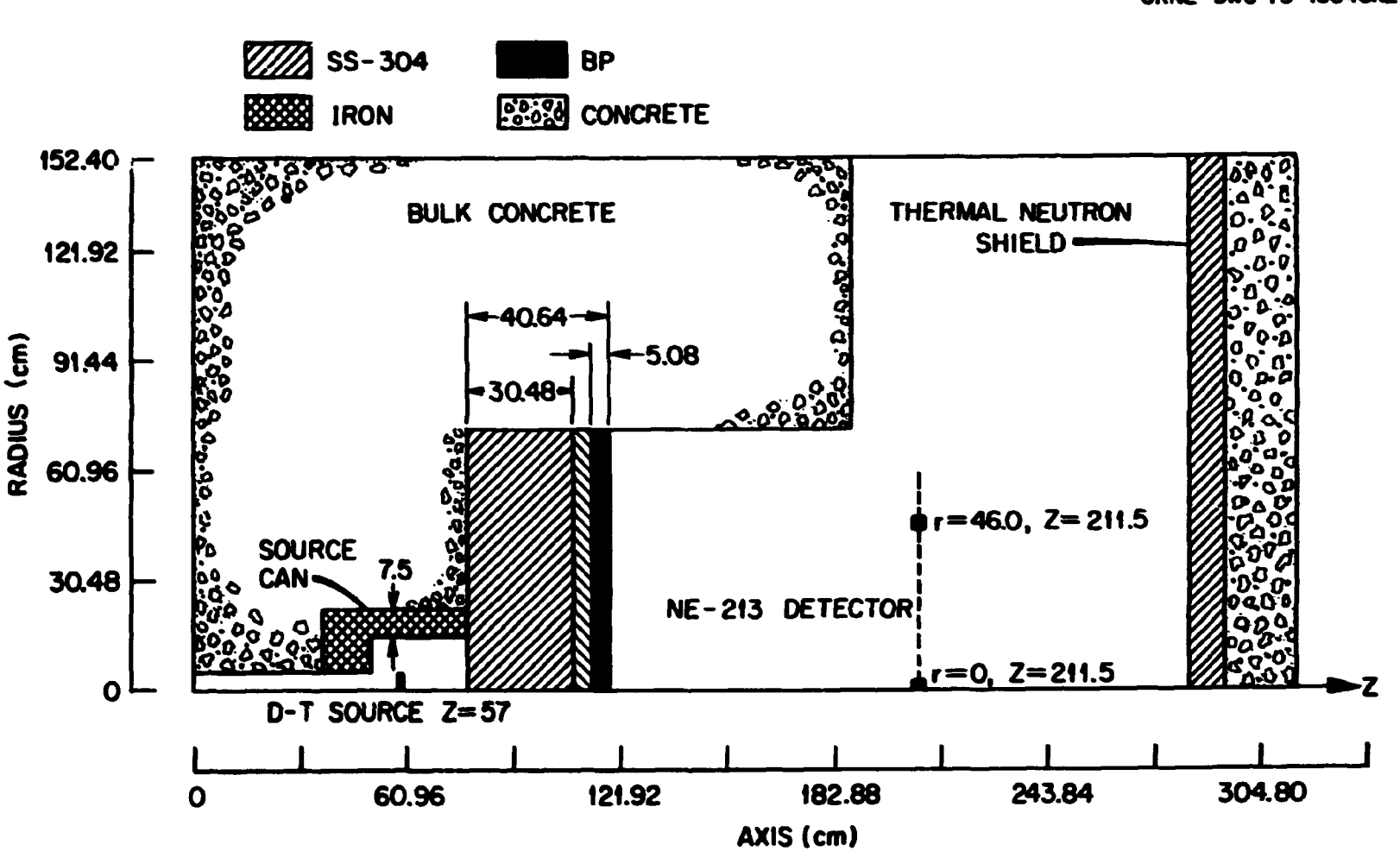

Fig. 1. Two-Dimensional Calculational Model of the Experimental Configuration.

intervals from the reactions of 250-keV deuterons in a 4-mg/cm^2-thick titanium-tritide target are given as a function of neutron energy in Table I.

Table I. Angle-Energy Dependence for Neutrons Emitted from the T(D,n)^{4}He Reaction

(Deuteron Energy = 250 keV)

Energy Interval (MeV)	Angular Interval 0.40°	40-180°
14.92-15.68	0.0130	
14.55-14.92	0.0902	0.0697
14.19-14.55	0.0168	0.2460
13.80-14.19		0.2913
13.50-13.80		0.2088
12.84-13.50		0.0642
Total	0.1200	0.8800

The source neutrons were angularly biased by specifying the probability for neutron emission into cones of fixed size. For the forward emitted neutrons, the cone angle θ, measured between the cone axis and the cone edge, was 40°. For the backward emitted neutrons, the cone angle was 140° (measured from the negative z axis). Particles were then sampled uniformly in the cone, $\cos\theta \leq w \leq 1$, with probability $p = 1$ (w is the direction cosine with z axis) and were assumed to be emitted from the target with an isotropic distribution in the cone. Neutrons having direction cosines u and v with the x and y axes, respectively, were not angularly biased.

The forward- and backward-emitted source neutrons were assigned weights W according to the relation $W = W' [(1-\cos\theta)/2p]$, where W' is the unbiased source particle weight. For the forward emitted source particles, $W_f = 0.1170\ W'$. For the backward-emitted source particles, $W_b = 0.8830\ W'$.

The source neutron energies were obtained by sampling uniformly within the energy intervals given in Table I according to the specified probabilities. To account for the anisotropy of particle emission into each cone, the probabilities for neutron production in the angle-energy intervals $P(\Delta E,\Delta\theta)$ were weighted using a solid angle factor given by

$$P_w(\Delta E,\Delta\theta) = \frac{2P(\Delta E,\Delta\theta)}{\int_{\theta_l}^{\theta} \sin\theta' d\theta'}$$

$$= \frac{P(\Delta E,\Delta\theta)}{W_l} \quad , \; l = f,b \; , \tag{4}$$

where $P_w(\Delta E,\Delta\theta)$ is the solid angle-weighted probability for neutrons in the energy interval ΔE and angular interval $\Delta\theta$ [as shown in Table I, P(ΔE, 0-40°) = 0.1200 and P(ΔE, 40° - 180°) = 0.8800]. Thus, to maintain the weighting according to the angle-energy dependence, the weights W_f and W_b are multiplied by the appropriate $P_w(\Delta E,\Delta\theta)$ given by Eq. (2).

The neutron flux at each detector position was obtained by combining the neutron fluxes calculated in the forward and backward analyses according to the relation

$$\phi_T^n(E) = \phi_{FU}^n(E) + \phi_{FC}^n(E) + \phi_{BC}^n(E) \; , \tag{5}$$

where

ϕ_T^n(E) = the total neutron flux at energy E per source neutron,

ϕ_{FU}^n(E) = the uncollided neutron flux at energy E per source neutron from neutrons emitted in the forward direction, and

ϕ_{FC}^n, ϕ_{BC}^n(E) = the collided neutron fluxes at energy E per source neutron from neutrons emitted in the forward and backward directions, respectively.

There is no contribution to the uncollided neutron flux at the detectors from neutrons emitted in the backward directions.

The gamma-ray flux was obtained using

$$\phi_T^\gamma(E) = \phi_F^\gamma(E) + \phi_B^\gamma(E) \; , \tag{6}$$

where

$\phi\gamma$ = the total gamma-ray flux at energy E per source neutron,

$\phi\gamma_F, \phi\gamma_B$ = the gamma-ray flux at energy E per source neutron produced by neutrons emitted in the forward and backward directions, respectively.

Russian roulette and particle splitting were used to reduce the variance of the calculated neutron and gamma-ray fluxes.

The MCNP calculations were carried out for three geometries: with the detectors 1.54 m from the source in an open geometry with no shielding material present, behind 0.154 m SS-304, and behind a laminated slab assembly containing 0.356 m SS-304, 0.051 m BP, 0.051 m SS-304, 0.051 m BP, and 0.051 m SS-304. ENDF/B-V transport cross sections were employed, and the compositions of the materials used in the calculations are given in Table II.

IV. DISCUSSION OF RESULTS

The differential neutron energy spectra calculated using the MCNP code are compared with the measured spectra and the calculated spectra from Refs. 2 and 3 in Figs. 2-4. In the figures, the solid curves are the measured spectra, the squares are the MCNP results, and the circles and triangles are the results from Refs. 2 and 3, respectively. [Note: The data from Ref. 3 are compared only for the differential neutron spectra. Gamma-ray spectra were not reported in Ref. 3.] The solid curves for each of the comparisons represent a 68% confidence interval in the measured spectra. The spectra calclated by MCNP have been smoothed by convoluting the neutron flux per unit energy with an energy-dependent Gaussian function having a width determined from Eq. (2). The MCNP data were initially binned into intervals having the same energy boundaries as the multigroup energy intervals used in the discrete ordinates calculations reported in Ref. 2. The error bars shown on the MCNP data indicate plus and minus one standard deviation in the estimated spectra. The MCNP Monte Carlo calculations were carried out using a sample size sufficient to obtain ±5% standard deviation in the unsmoothed neutron flux per unit energy above 10 MeV. The data from Ref. 3 were smoothed in the same manner as that used in this work, but since the unsmoothed energy intervals had different energy boundaries than those used here, the smoothed data are shifted slightly in energy. The error bars given with the spectra from Ref. 3 have been omitted in the figures to avoid confusion, but they are comparable with those obtained for the MCNP spectra.

Table II. Composition of Materials Used in the Calculation

	Composition (atom/cm·Barn)				
Element	**Concrete**	**Air**	**Source Can**	**SS-304**	**BP***
H	7.86(-3)+				7.13(-2)
B-10					4.87(-4)
B-11					1.97(-3)
C					3.41(-2)
N		3.64(-5)			
O	4.39(-2)	9.74(-6)			3.64(-3)
Na	1.05(-3)				
Mg	1.40(-4)				
Al	2.39(-3)				
Si	1.58(-2)				
K	6.90(-4)				
Ca	2.92(-3)				
Cr				1.77(-2)	
Mn				1.77(-3)	
Fe	3.10(-4)			6.02(-2)	
Ni				7.83(-3)	

*BP = Borated Polyethylene.

+Read as 7.86×10^{-3}.

Figure 2 compares the measured and calculated differential neutron energy spectra for neutrons with energies above 850 keV for the case with the detector on the axis of symmetry and with no shielding material in the cavity in the concrete experiment support structure (see Fig. 1). The source-to-detector distance is 1.54 m. The spectrum calculated using the MCNP code is in good agreement with the measured spectrum at all neutron energies and compares very favorably with the calculated spectra reported in Refs. 2 and 3. For all of the spectra, the neutron flux above ~12 MeV is dominated by neutrons emitted directly from the D-T source. The spectrum at lower energies arises principally from neutrons scattered from the concrete structure. The agreement between the calculated and measured neutron spectra for this open geometry provides verification of the procedures used to represent the angle-energy dependent D-T neutron source distribution in the calculations.

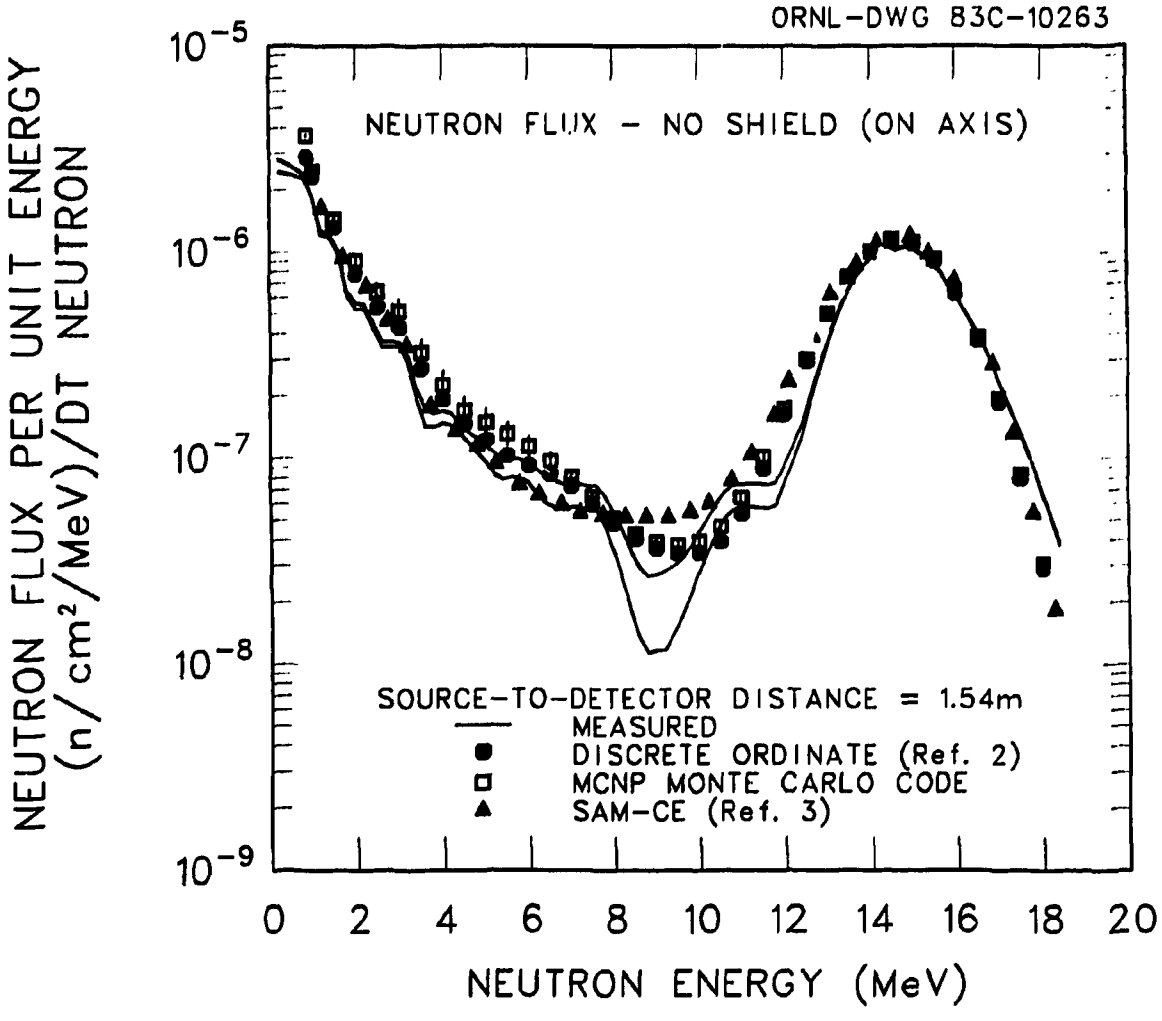

Fig. 2. Neutron Flux Per Unit Energy Versus Neutron Energy for the Detector On Axis at a Source-to-Detector Distance of 1.54 m. No shielding material present.

Figure 3 shows the comparisons between the measured and calculated differential neutron energy spectra for the case with the detector on the axis of symmetry behind both a 0.152-m-thick SS-304 slab and also behind a laminated slab assembly containing 0.457 m SS-304 and 0.102 m BP. The source-to-detector distance is 1.54 m. The spectrum calculated using the MCNP code is in good agreement with the measured spectrum at all neutron energies. At neutron energies above ~11 MeV, the MCNP data agree more favorably with the measured data than do the discrete ordinates results. Between ~8 and ~11 MeV, the MCNP spectrum is in good agreement with the measured spectrum, whereas the discrete ordinates spectrum overpredicts the measured data. The spectra calculated using both MCNP and SAM-CE agree with the measured data and with each other at neutron energies above ~8 MeV. At neutron energies between ~2 and ~8 MeV, the spectrum calculated using SAM-CE[3] falls slightly below both the measured and MCNP data.

For the shield assembly comprised of 0.457 m SS-304 and 0.02 m BP, the spectrum calculated with MCNP is in very favorable agreement with the measured spectrum and also with the calculated data from Ref. 2. The spectrum calculated using SAM-CE shows a slight deviation from the measured data at neutron energies between ~6 and ~11 MeV and is also in slight disagreement at these energies with the MCNP results obtained here and with the discrete ordinates data from Ref. 2.

Figure 4 shows the comparisons between the measured and calculated differential neutron spectra for the case with the detector off the axis of symmetry behind the SS-304 and SS-304 plus BP shield assemblies described above. The source-to-detector distance along the z-axis is 1.54 m and the detector is at r = 0.46 m (see Fig. 1). The spectra calculated using MCNP reproduce the measured spectra fairly well over all neutron energies for both shield assemblies. At neutron energies above ~12 MeV the MCNP data are higher than the measured spectra particularly behind the 0.152-m-thick SS-304 shield. For this case, the MCNP data are also higher than the calculated data from Refs. 2 and 3. The discrete ordinates calculation, in fact, underestimates the neutron flux in the peak of spectrum. For the thick shield assembly, MCNP reproduces the measurement in the peak within statistics and the calculated data from all methods are in good agreement with each other. At neutron energies below ~12 MeV, the spectra calculated using MCNP are in good agreement with the measured data and those from Ref. 2 for both slab assemblies.

The measured and calculated energy integrated neutron spectra for the three cases discussed above are shown in Figs. 5-7. In these figures, only the MCNP and discrete ordinates integral data from Ref. 2 are compared with the measured data. For the case of the detector on-axis and no shield material present, the integral spectrum calculated with MCNP shown in Fig. 5 is in good agreement with the measured spectrum and that calculated in Ref. 2. The MCNP spectrum reproduces the measured result to better than 10% at all neutron energies. The energy integrated spectra calculated with MCNP for the detector on and off the axis and behind shield assemblies comprised of 0.152 m SS-304 or 0.457 m SS-304 plus 0.102 m BP are compared with the measured spectra and those from Ref. 2 in Figs. 6 and 7, respectively. The MCNP energy integrated neutron spectra are slightly higher ($\leq$20%) than the measured spectra at both detector locations and behind both shield assemblies compared in the figures.

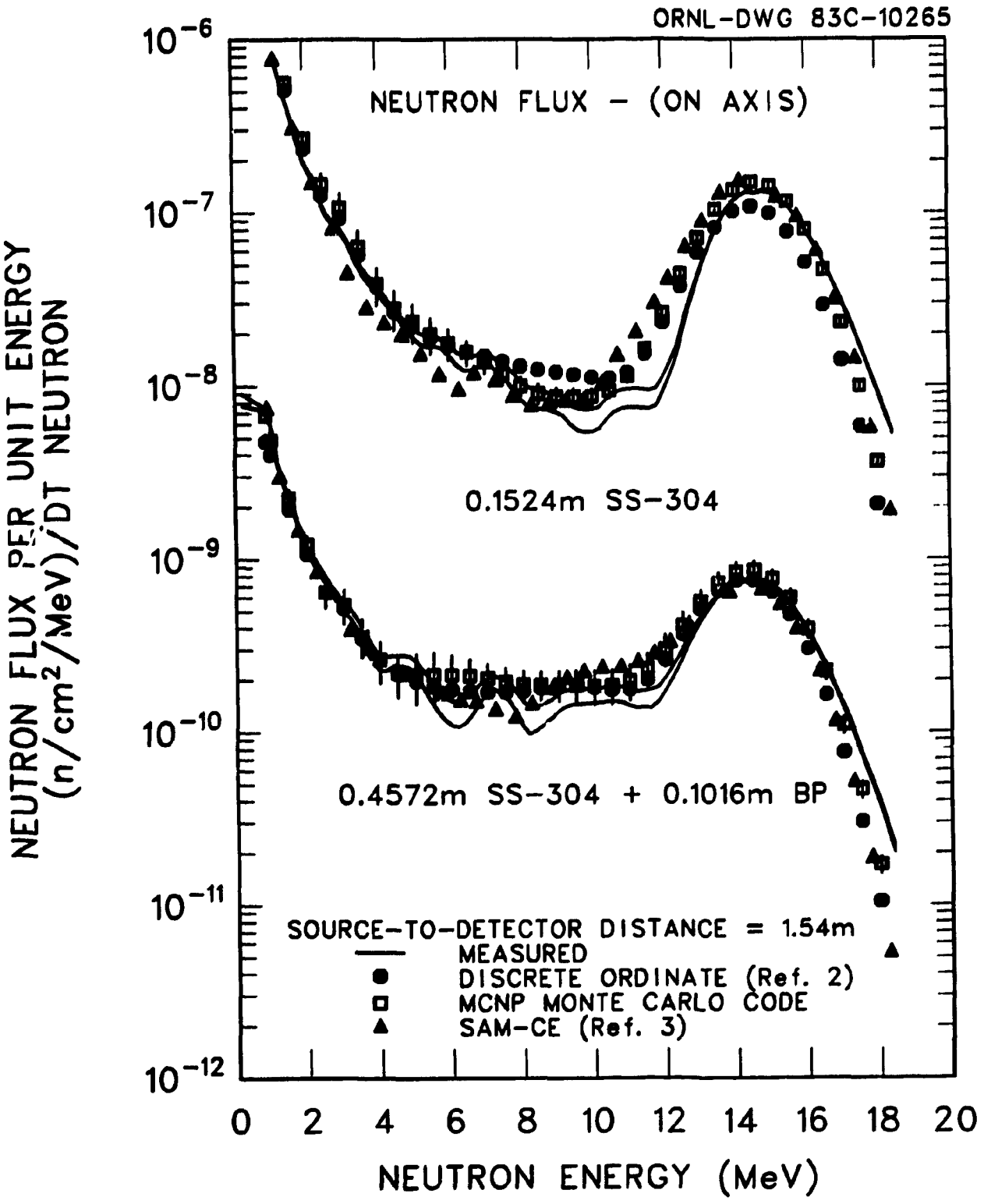

Fig. 3. Neutron Flux Per Unit Energy Versus Neutron Energy for the Detector On Axis at a Source-to-Detector Distance of 1.54 m for Shield Configurations with 0.152 m SS-304 and 0.457 m SS-304 Plus 0.102 m Borated Polyethylene.

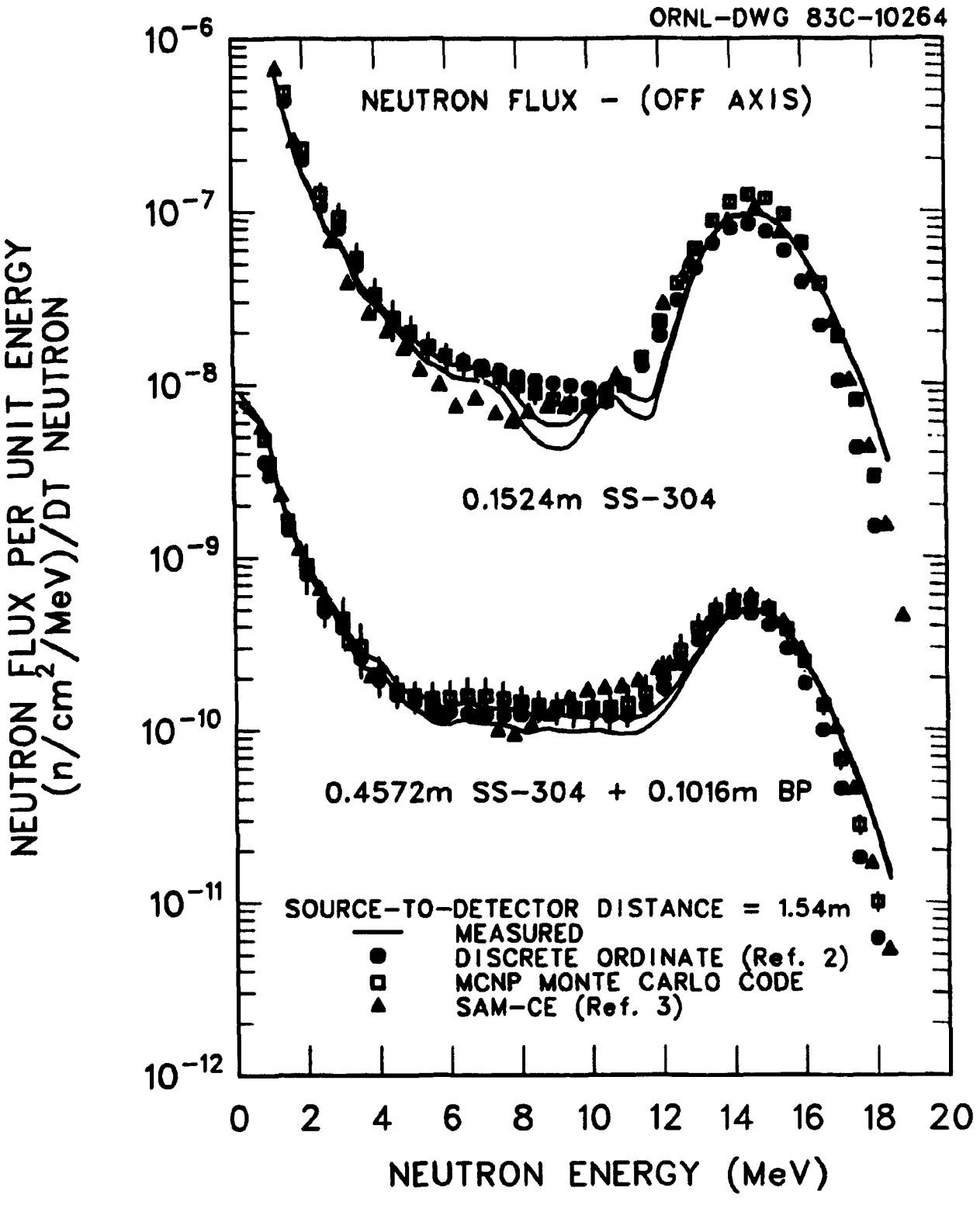

Fig. 4. Neutron Flux Per Unit Energy Versus Neutron Energy for the Detector Off Axis (r= 0.46 m) at a Source-to-Detector Distance Along the Z-Axis of 1.54 m for Shield Configurations with 0.152 m SS-304 and 0.457 m SS-304 Plus 0.102 m Borated Polyethylene.

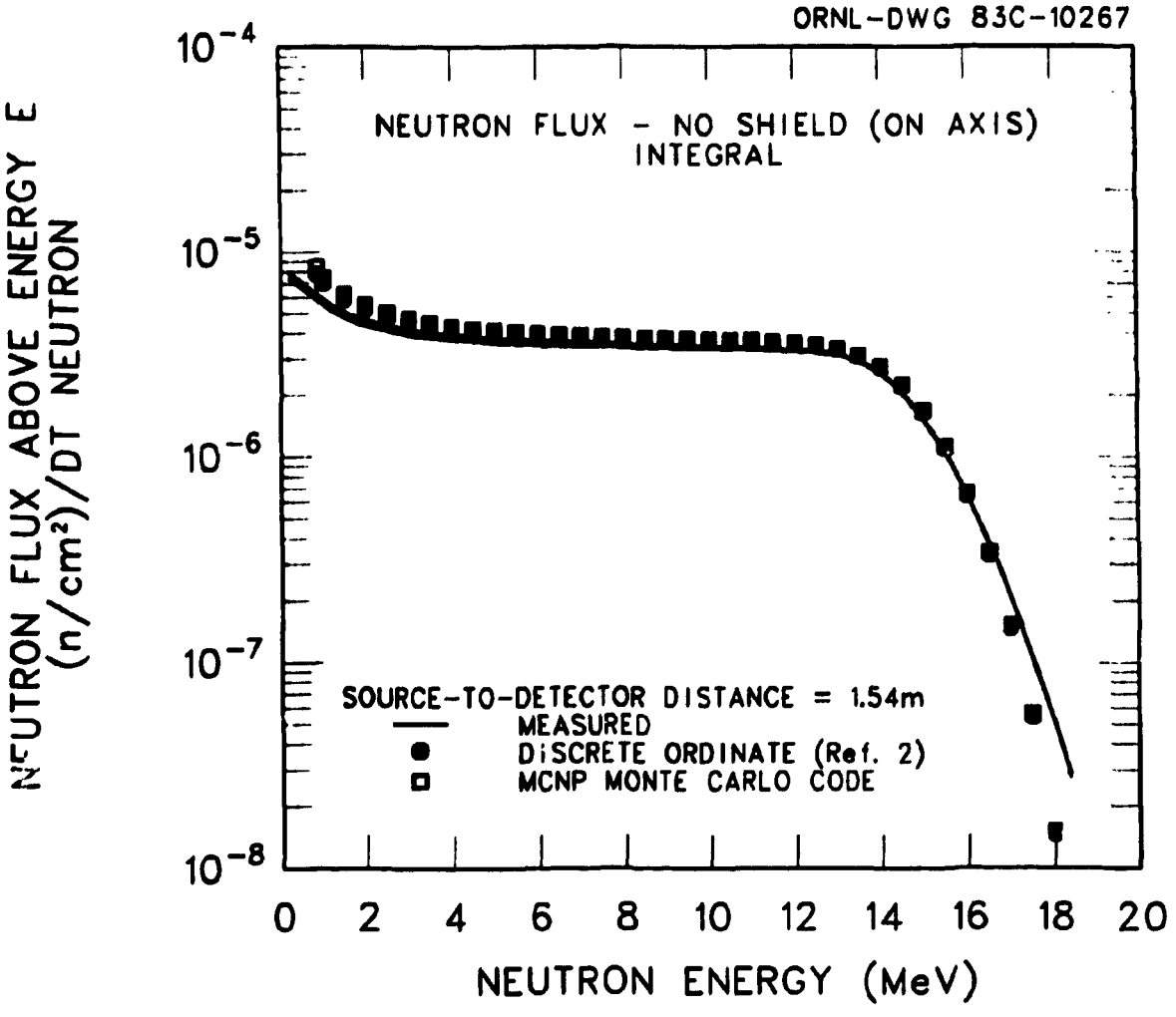

Fig. 5. Neutron Flux Above Energy E Versus Neutron Energy for the Detector On Axis at a Source-to Detector Distance of 1.54 m. No shielding material present.

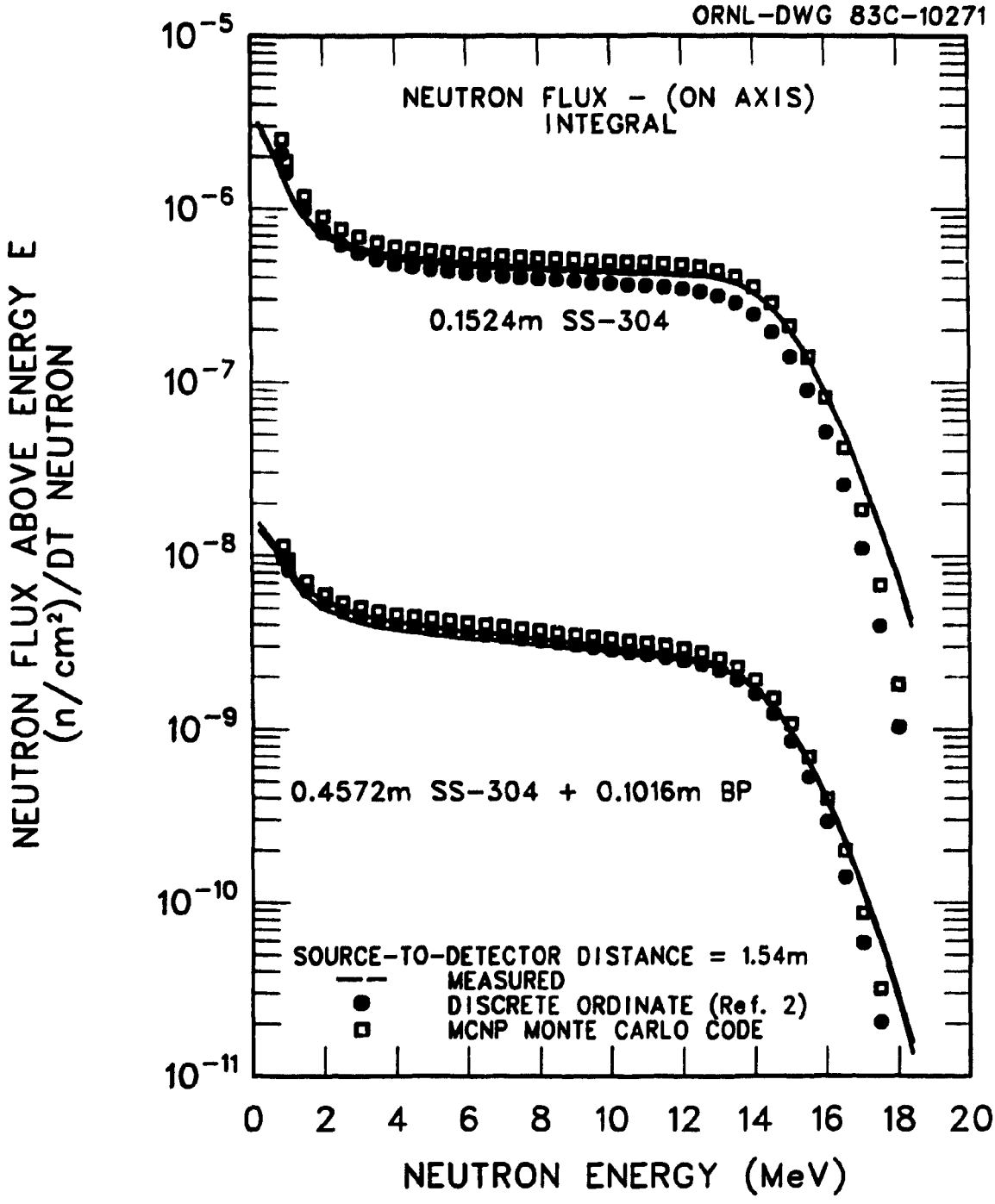

Fig. 6. Neutron Flux Above Energy E Versus Neutron Energy for the Detector On Axis at a Source-to-Detector Distance of 1.54 m for Shield Configurations with 0.152 m SS-304 and 0.457 m SS-304 Plus 0.102 m Borated Polyethylene.

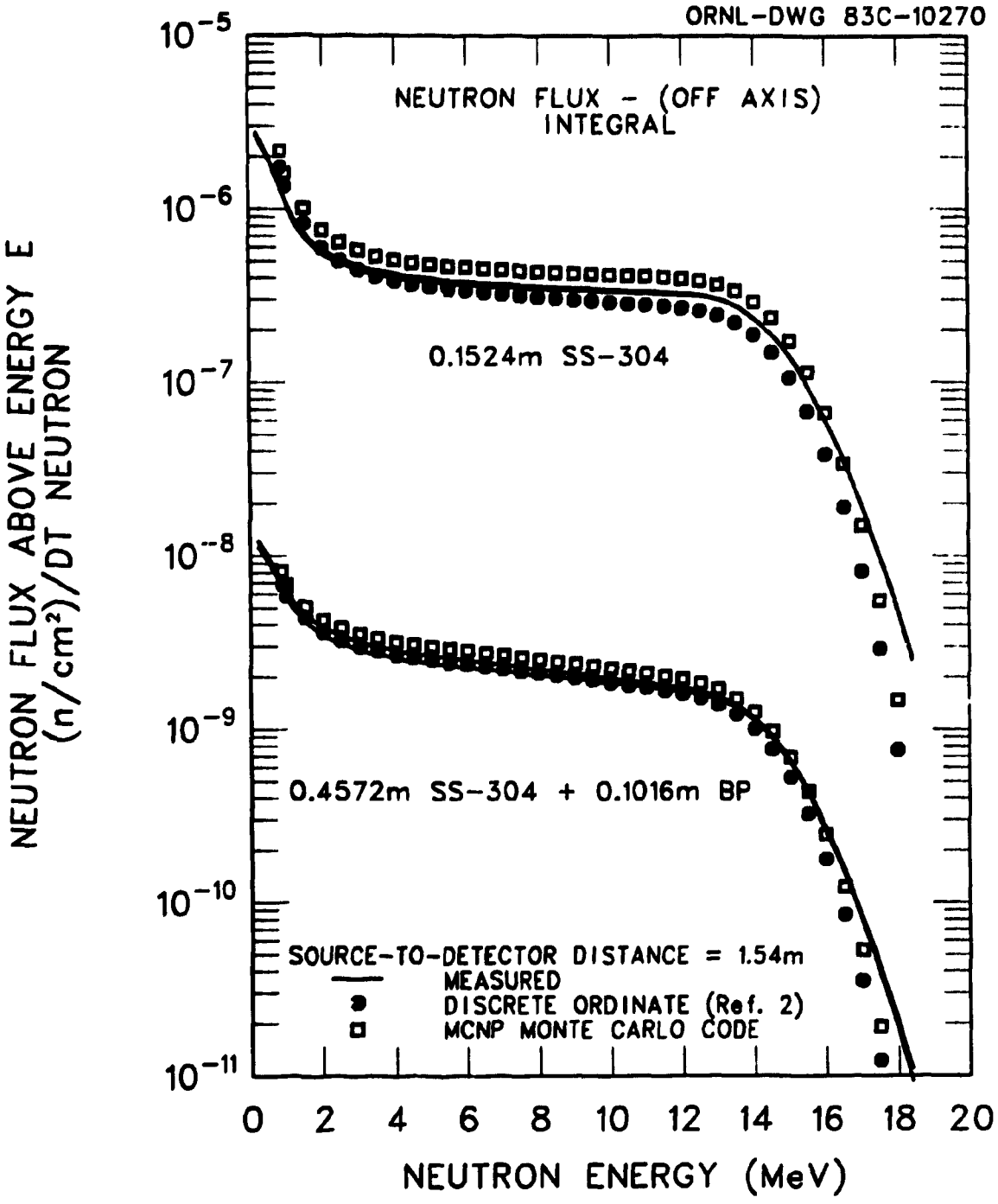

Fig. 7. Neutron Flux Above Energy E Versus Neutron Energy for the Detector Off Axis (r = 0.46 m) at a Source-to-Detector Distance Along the Z-Axis of 1.54 m for Shield Configurations with 0.152 m SS-304 and 0.457 m SS-304 Plus 0.102 m Borated Polyethylene.

Figures 8-11 show the comparison between the measured and calculated differential and integral gamma-ray energy spectra, respectively. In these figures, the calculated gamma-ray data are from the MCNP Monte Carlo calculation and from the discrete ordinates calculation reported in Ref. 2. No gamma-ray spectra were calculated by the authors of Ref. 3. The MCNP code reproduces the differential data in magnitude, but not in shape. The coarse energy grid used to bin the gamma-ray data apparently washes out the line structure. The agreement between the MCNP results and those from Ref. 2 is also favorable. The energy integrated gamma-ray energy spectra using MCNP are also in good agreement with the measured spectra and those calculated in Ref. 2.

CONCLUSIONS

The results obtained here suggest that Monte Carlo radiation transport methods that utilize continuous cross-section data and appropriate source sampling procedures will provide a useful tool for analyzing 14-MeV neutron processes and attenuation in fusion reactor shields. The differences among the calculated data compared here are acceptably small and suggest that the selection of the method of analysis depends mainly on problem geometry and the goals of the analysis.

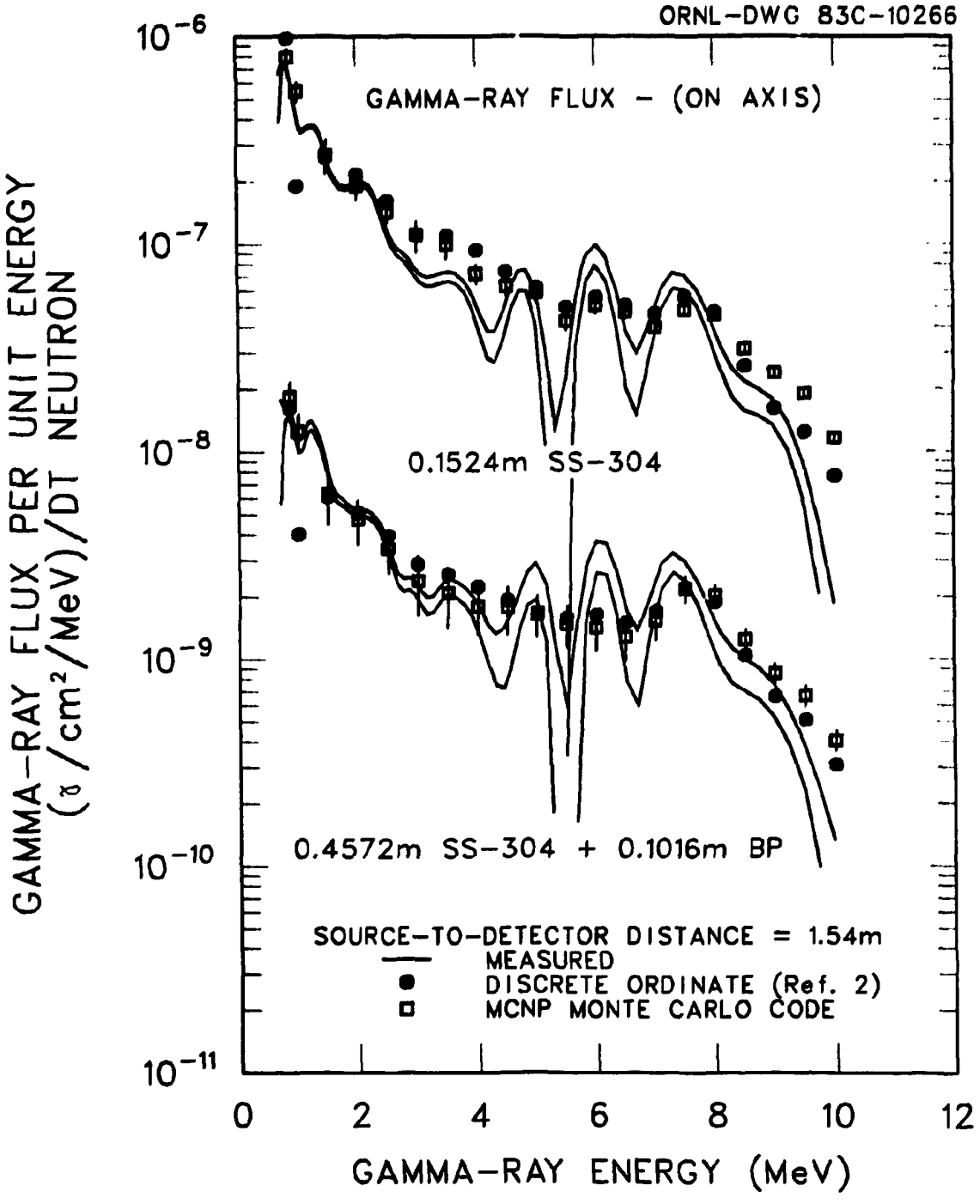

Fig. 8. Gamma Ray Flux Per Unit Energy Versus Gamma Ray Energy for the Detector On Axis at a Source-to-Detector Distance of 1.54 m for Shield Configurations with 0.152 m SS-304 and 0.457 m SS-304 Plus 0.102 m Borated Polyethylene.

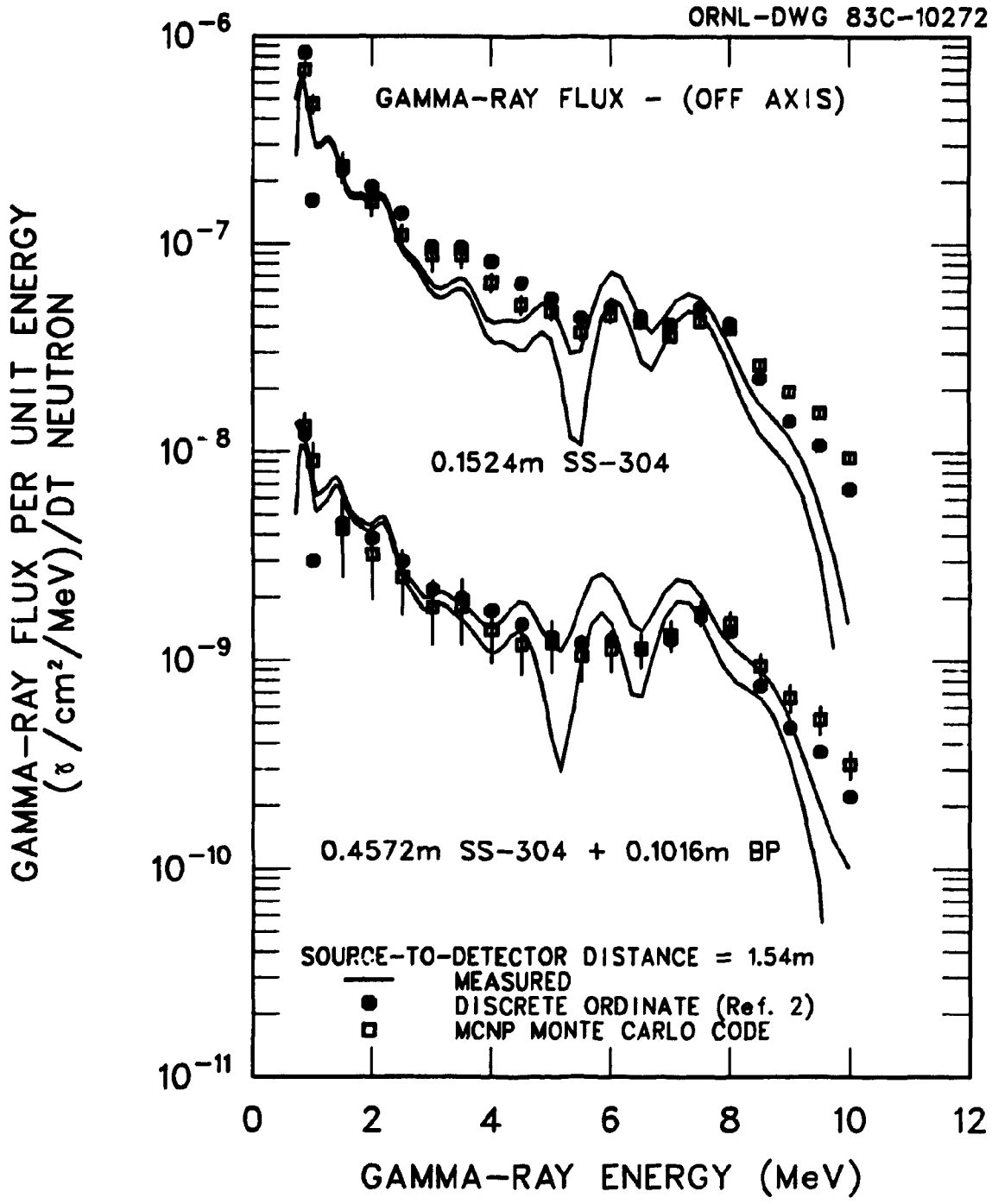

Fig. 9. Gamma Ray Flux Per Unit Energy Versus Gamma-Ray Energy for the Detector Off Axis (r = 0.46 m) at a Source-to-Detector Distance Along the Z-Axis of 1.54 m for Shield Configurations with 0.152 m SS-304 and 0.457 m SS-304 Plus 0.102 m Borated Polyethylene.

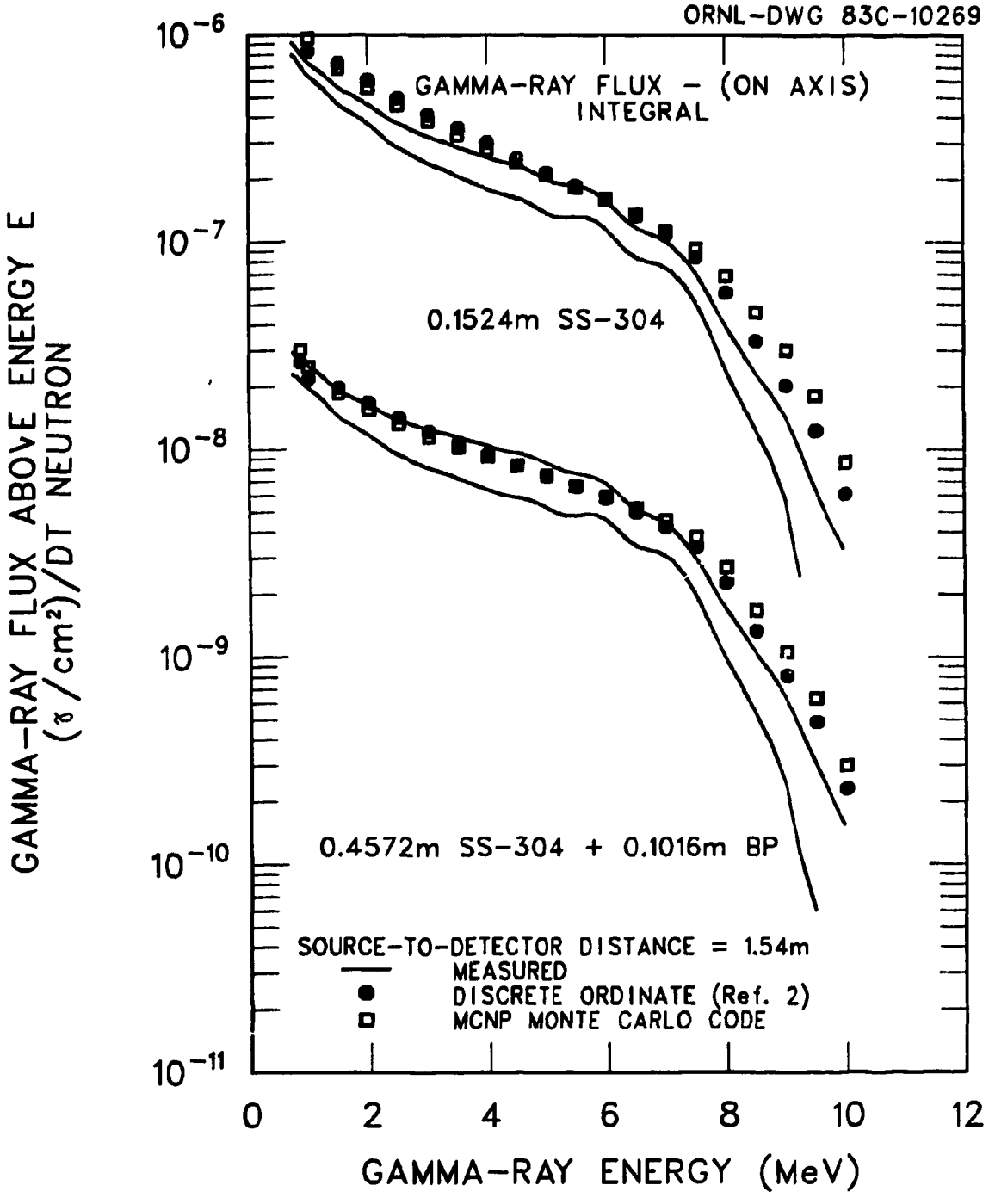

Fig. 10. Gamma Ray Flux Above Energy E Versus Gamma-Ray Energy for the Detector On Axis at a Source-to-Detector Distance of 1.54 m for Shield Configurations with 0.152 m SS-304 and 0.457 m SS-304 Plus 0.102 m Borated Polyethylene.

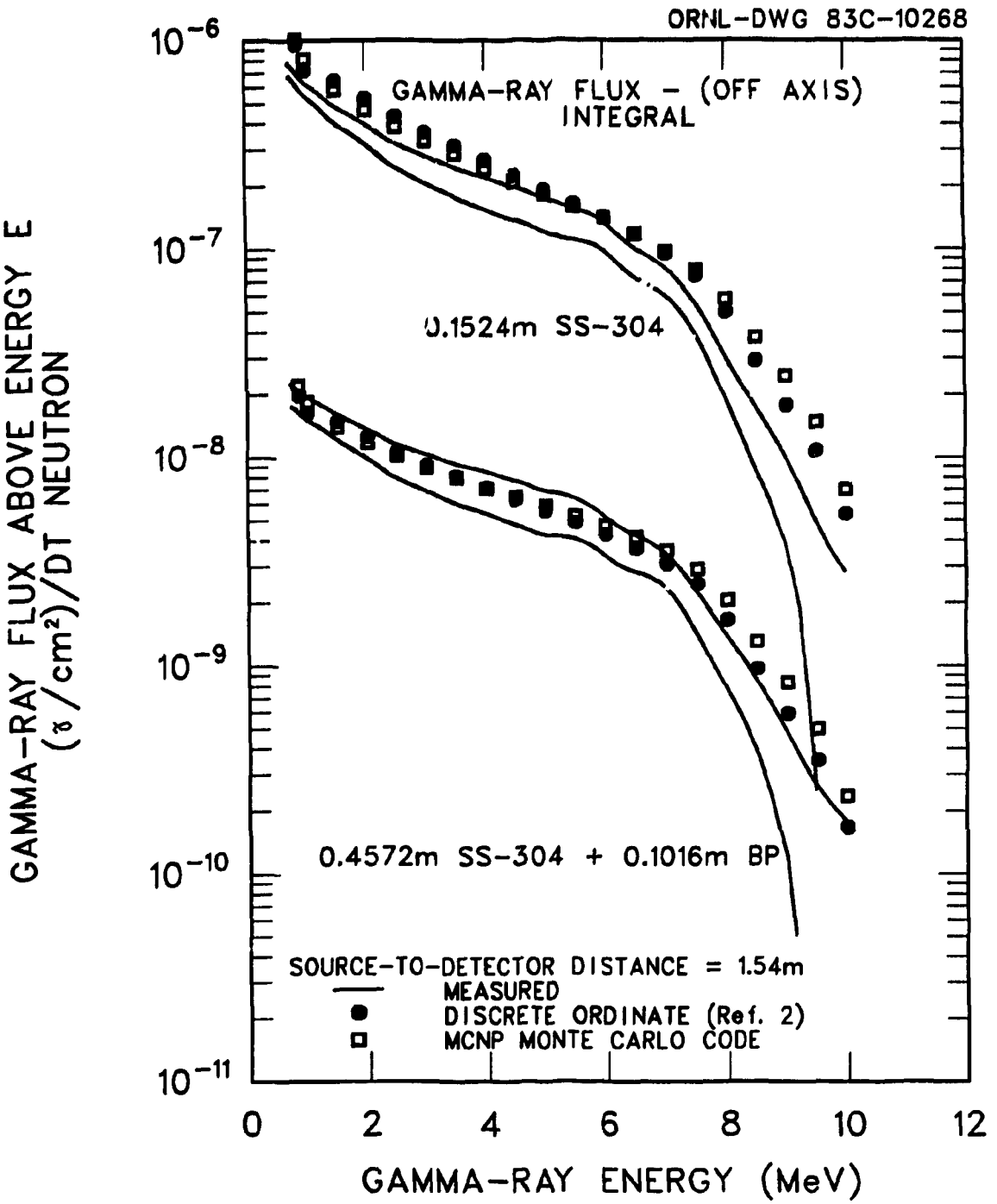

Fig. 11. Gamma Ray Flux Above Energy E Versus Gamma Ray Energy for the Detector Off Axis (r = 0.46 m0 at a Source-to-Detector Distance Along the Z-Axis of 1.54 m for Shield Configurations with 0.152 m SS-304 and 0.457 m SS-304 Plus 0.102 m Borated Polyethylene.

REFERENCES

1. "MCNP - A General Purpose Monte Carlo Code for Neutron and Photon Transport," LA-7396-M, (Rev) Version 2B, Los Alamos Monte Carlo Group, Los Alamos National Laboratory (1981).
2. R. T. SANTORO, R. G. ALSMILLER, JR., J. M. BARNES, G. T. CHAPMAN, *Nucl. Sci. Eng. 78*, 259 (1981).
3. E. SCHMIDT and P. ROSE, "Monte Carlo Calculation of a Fusion Reactor Experiment," to be published in *Nucl. Sci. Eng.*
4. R. T. SANTORO, J. M. BARNES, R. G. ALSMILLER, JR., and E. M. OBLOW, "Calculational Procedures for the Analysis of Integral Experiments for Fusion Reactor Design," ORNL-5777, Oak Ridge National Laboratory (1981).
5. W. R. BURRIS and V. V. VERBINKSI, *Nucl. Instr. Methods 67*, 181 (1979).
6. G. T. CHAPMAN, G. L. MORGAN, and J. W. MCCONNELL, "The ORNL Integral Experiment to Provide Data for Evaluating Magnetic Fusion Energy Shielding Concepts Part 1: Attenuation Measurements," ORNL/TM-7356, Oak Ridge National Laboratory (1982).

ORNL/TM-8707
Distribution Category UC-20d

INTERNAL DISTRIBUTION

1–3. L. S. Abbott
4. F. S. Alsmiller
5–9. R. G. Alsmiller, Jr.
10–14. J. M. Barnes
15. D. E. Bartine
16. G. T. Chapman
17–20. EPD Reports Office
21. W. E. Ford, III
22. T. A. Gabriel
23. R. A. Lillie
24. J. L. Lucius
25. F. C. Maienschein
26. R. W. Peelle
27. R. W. Roussin
28. M. W. Rosenthal
29. RSIC
30. M. J. Saltmarsh
31–35. R. T. Santoro
36. D. Steiner
37. C. R. Weisbin
38. A. Zucker
39. P. W. Dickson, Jr. (Consultant)
40. H. J. C. Kouts (Consultant)
41. W. B. Loewenstein (Consultant)
42. R. Wilson (Consultant)
43–44. Central Research Library
45. Fusion Energy Division Library
46. Fusion Energy Division Reports Office
47. ORNL Y-12 Technical Library Document Reference Section
48–49. Laboratory Records
50. ORNL Patent Office
51. Laboratory Records - RC

EXTERNAL DISTRIBUTION

52. Office of Assistant Manager for Energy Research & Development, DOE-ORO, Oak Ridge, TN 37830.

53. J. E. Baublitz, Office of Fusion Energy, Division of Development and Technology, MS G-234, U.S. Dept. of Energy, Washington, D.C. DC 20545.

54. S. E. Berk, Division of Development and Technology, Office of Fusion Energy, ER-532, U.S. Dept. of Energy, Washington, D.C. 20545.

55. J. D. Callen, Dept. of Nuclear Engineering, University of Wisconsin Madison, WI 53706.

56. R. W. Conn, Dept. of Chemical, Nuclear and Thermal Engineering, University of California, Los Angeles, CA 90024.

57. S. O. Dean, Director, Fusion Energy Development, Science Applications, Inc., 2 Professional Dr., Suite 249, Gaithersburg, MD 20760.

58. B. Engholm, General Atomic Co., P.O. Box 81608, San Diego, CA 92138.

59. H. K. Forsen, Bechtel Group, Inc., Research Engineering, P.O. Box 3964, San Francisco, CA 94105.

60. R. W. Gould, Dept. of Applied Physics, California Institute of Technology, Pasadena, CA 92024.

61. D. G. McAlees, Exxon Nuclear Co., Inc., 777 106th Ave., N.E., Bellevue, WA 98009.

62. P. J. Reardon, Princeton Plasma Physics Laboratory, Princeton University, P.O. Box 451, Princeton, NJ 08540.

63. P. Sager, General Atomic Co., P.O. Box 81608, San Diego, CA 92138.

64. W. M. Stacey, Jr., School of Nuclear Engineering, Georgia Institute of Technology, Atlanta, GA 30332.

EXTERNAL - FOREIGN

65. Bibliothek, Institut fur Plasmaphysik, D-8046, Garching bei Munchen, Federal Republic of Germany.

66. Bibliothek, Institut fur Plasmaphysik, KFA, Postfach 1913, D-5170, Julich 1, Federal Republic of Germany.

67. Bibliotheque, Service du Confinement des Plasmas, CEA, B.P. No. 6, 92, Fontenay aux Roses (Seine), France.

68. Documentation, S.I.G.N., D.P.PFC. CEN, P.O. 85, Centre de Tri, 38041 Cedex, Grenoble, France.

69. Institute of Physics, Academia Sinica, Peking, Peoples Republic of China.

70. Library, Centre de Recherches en Physique des Plasmas, 21 Avenue des Bains, 1007, Lausanne, Switzerland.

71. Library, Culham Laboratory, UKAEA, Abingdon, Oxon, OX.4-3DB, England.

72. Library, FOM Institute voor Plasma-Fysica, Rijnhuizen, Jutphass, Netherlands.

73. Library, Institute for Plasma Physics, Nagoya University, Nagoya 464, Japan.

74. Library, International Centre for Theoretical Physics, Trieste, Italy.

75. Library, Laboratoria Gas Ionizzati, Frascati, Italy.

76. Library, Plasma Physics Laboratory, Kyoto University, Gokasho Uji, Kyoto, Japan.

77. Plasma Research Laboratory, Australian National University, P.O. Box 4, Canberra ACT.2000, Australia.

78. Dr. Yasushi Seki, Japan Atomic Energy Research Institute, Tokai-mura, Ibaraki-ken, Japan.

79. Thermonuclear Library, Japan Atomic Energy Research Institute, Tokai, Naka, Ibaraki, Japan.

80. R. Varma, Physical Research Laboratory, Navangpura, Ahmedabad, India.

81. Dr. Michinori Yamauchi, Nippon Atomic Industry Group Co., Ltd., NAIG Nuclear Research Laboratory, 4-1, Ukishima-cho, Kawasaki-ku, Kawasaki City, 210, Japan.

82–211. Given distribution as shown in TID-4500, Magnetic Fusion Energy (Distribution Category UC-20d: Fusion Systems).